Available online at www.sciencedirect.com
SCIENCE DIRECT
Trans. Nonferrous Met. Soc. China 16(2006) 1362−1369
Transactions of Nonferrous Metals Society of China
www.csu.edu.cn/ysxb/

Effects of constitutive parameters on adiabatic shear localization for ductile metal based on JOHNSON-COOK and gradient plasticity models

WANG Xue-bin(王学滨)

Department of Mechanics and Engineering Sciences, Liaoning Technical University, Fuxin 123000, China

Received 6 March 2006; accepted 8 May 2006

Abstract: By using the widely used JOHNSON-COOK model and the gradient-dependent plasticity to consider microstructural effect beyond the occurrence of shear strain localization, the distributions of local plastic shear strain and deformation in adiabatic shear band(ASB) were analyzed. The peak local plastic shear strain is proportional to the average plastic shear strain, while it is inversely proportional to the critical plastic shear strain corresponding to the peak flow shear stress. The relative plastic shear deformation between the top and base of ASB depends on the thickness of ASB and the average plastic shear strain. A parametric study was carried out to study the influence of constitutive parameters on shear strain localization. Higher values of static shear strength and work to heat conversion factor lead to lower critical plastic shear strain so that the shear localization is more apparent at the same average plastic shear strain. Higher values of strain-hardening exponent, strain rate sensitive coefficient, melting point, thermal capacity and mass density result in higher critical plastic shear strain, leading to less apparent shear localization at the same average plastic shear strain. The strain rate sensitive coefficient has a minor influence on the critical plastic shear strain, the distributions of local plastic shear strain and deformation in ASB. The effect of strain-hardening modulus on the critical plastic shear strain is not monotonous. When the maximum critical plastic shear strain is reached, the least apparent shear localization occurs.

Key words: adiabatic shear band; ductile metal; shear localization; JOHNSON-COOK model; constitutive parameters

1 Introduction

Adiabatic shear band(ASB) is a very narrow zone with a high concentration of shear strain. It is believed that ASB is formed by a process of thermo-mechanical instability. ASB can be observed in the process of dynamic deformation of various ferrous and nonferrous metals (such as titanium, aluminum and steels), alloys (such as titanium alloys, aluminum alloys and metallic glass), single crystals, polycrystals, polymers and geomaterials (such as rock and soil).

The various problems related to ASB were studied by experimental tests[1−11], numerical simulations [9,12−14] and theoretical analyses[1,9,15], such as the critical conditions for ASB formation, the sites for initiation of ASB, the propagation of ASB, the microstructural characteristics in ASB and outside, the nucleation, growth and coalescence of voids and microcracks in ASB, the length, number, width, spacing, pattern, orientation of ASB, the development or evolution of stress, strain, strain rate, deformation and temperature in ASB.

Different from the previous investigations, on the aspect of theoretical analysis, the work by WANG et al [16−22] was focused on the distributions of plastic strain, deformation, temperature and damage variable in ASB based on gradient-dependent plasticity where an internal length parameter was included in the yield function to describe the interactions and interplay among microstructures in ductile metals, such as titanium and its alloys as well as low-carbon steel. Considering the effects of strain-hardening, strain-rate sensitivity, thermal-softening and microstructures, JOHNSON-COOK model and gradient-dependent plasticity were used to calculate the temperature distribution in ASB[22].

In this study, by using the widely used JOHNSON-COOK model and the gradient-dependent plasticity to consider microstructural effect beyond the occurrence of shear strain localization, the characteristics of local plastic shear strain and deformation in ASB are analyzed. A detailed parametric study is carried out to study the influence of constitutive parameters on the flow shear

Foundation item: Project(2004F052) supported by the Education Department of Liaoning Province, China
Corresponding author: WANG Xue-bin; Tel: +86-418-3351351; E-mail: wxbbb@263.net

stress-average plastic shear strain curve, the critical plastic shear strain, the distributions of local plastic shear strain and deformation in ASB.

2 JOHNSON-COOK model and initiation of shear localization

In JOHNSON-COOK model[13], the flow shear stress τ and the temperature T are

$$\tau=\left(A+B\bar{\gamma}_{\mathrm{p}}^{n}\right)\cdot\left(1+C\ln\frac{\dot{\gamma}}{\dot{\gamma}_0}\right)\cdot\left[1-\left(\frac{T-T_0}{T_{\mathrm{m}}-T_0}\right)^{m}\right] \tag{1}$$

$$T=T_0+\frac{\beta}{\rho c_p}\int\tau\,\mathrm{d}\bar{\gamma}_{\mathrm{p}} \tag{2}$$

where $\bar{\gamma}_{\mathrm{p}}$ is the average plastic shear strain; $\dot{\gamma}_0$ is the reference shear strain rate; $\dot{\gamma}$ is the imposed shear strain rate; T_0 is the initial temperature; T_{m} is the melting temperature; β is the work to heat conversion factor; c_p is the heat capacity; ρ is the density; A, B, C, m, and n are static shear strength, strain-hardening modulus, strain rate sensitive coefficient, thermal-softening exponent and strain-hardening exponent, respectively.

The occurrence of ASB is usually attributed to the thermal-plastic shear instability: the thermal softening due to the dissipation of part of the mechanical work just overcomes the strain-hardening effect. Therefore, the condition for the onset of ASB is

$$\mathrm{d}\tau=0 \tag{3}$$

where d is a differential sign.

Average plastic shear strain corresponding to the peak flow shear stress $\tau_{\max}$ is called the critical plastic shear strain γ_{c}.

In the strain-hardening stage prior to the peak stress $\tau_{\max}$, there is

$$\mathrm{d}\tau<0 \tag{4}$$

In the strain-softening stage beyond the occurrence of ASB, there is

$$\mathrm{d}\tau>0 \tag{5}$$

3 Analysis of characteristics of local plastic shear strain and deformation in ASB

Using gradient-dependent plasticity, WANG[22] derived the thickness w of ASB and the distribution $\gamma_{\mathrm{p}}(y)$ of local plastic shear strain in ASB:

$$w=2\pi l \tag{6}$$

$$\gamma_{\mathrm{p}}(y)=\gamma_{\mathrm{c}}+\left(\bar{\gamma}_{\mathrm{p}}-\gamma_{\mathrm{c}}\right)\cdot\left(1+\cos\frac{y}{l}\right) \tag{7}$$

where l is the internal length parameter reflecting the heterogeneous extent of ductile metal material; y is the coordinate whose original point is set at the center of ASB.

We can determine the maximum value of $\gamma_{\mathrm{p}}(y)$ using Eqn.(7):

$$\gamma_{\mathrm{p,max}}=\gamma_{\mathrm{p}}(0)=\gamma_{\mathrm{c}}+2\left(\bar{\gamma}_{\mathrm{p}}-\gamma_{\mathrm{c}}\right) \tag{8}$$

The minimum value of $\gamma_{\mathrm{p}}(y)$ is reached at the two boundaries of ASB:

$$\gamma_{\mathrm{p,min}}=\gamma_{\mathrm{p}}\left(\pm\frac{w}{2}\right)=\gamma_{\mathrm{c}} \tag{9}$$

The first-order gradient of $\gamma_{\mathrm{p}}(y)$ with respect to the coordinate y is

$$\frac{\mathrm{d}\gamma_{\mathrm{p}}(y)}{\mathrm{d}y}=-\frac{1}{l}\sin\frac{y}{l}\cdot\left(\bar{\gamma}_{\mathrm{p}}-\gamma_{\mathrm{c}}\right) \tag{10}$$

When

$$y\in\left(-\frac{w}{2},0\right),\quad\frac{\mathrm{d}\gamma_{\mathrm{p}}(y)}{\mathrm{d}y}>0$$

When

$$y\in\left[0,\frac{w}{2}\right),\quad\frac{\mathrm{d}\gamma_{\mathrm{p}}(y)}{\mathrm{d}y}\le 0$$

Using Eqns.(8) and (9), we can establish the relation for the nonlocal variable $\bar{\gamma}_{\mathrm{p}}-\gamma_{\mathrm{c}}$:

$$\bar{\gamma}_{\mathrm{p}}-\gamma_{\mathrm{c}}=\frac{1}{2}\left(\gamma_{\mathrm{p,max}}-\gamma_{\mathrm{p,min}}\right) \tag{11}$$

According to the geometrical equation (the relation between strain and deformation), the local plastic shear strain $\gamma_{\mathrm{p}}(y)$ is related to the local plastic shear deformation $s_{\mathrm{p}}(y)$:

$$\gamma_{\mathrm{p}}(y)=\frac{\mathrm{d}s_{\mathrm{p}}(y)}{\mathrm{d}y} \tag{12}$$

Thus, $s_{\mathrm{p}}(y)$ is expressed as

$$s_{\mathrm{p}}(y)=\int_0^y\gamma_{\mathrm{p}}(y)\mathrm{d}y=\gamma_{\mathrm{c}}y+\left(\bar{\gamma}_{\mathrm{p}}-\gamma_{\mathrm{c}}\right)\cdot\left(y+l\sin\frac{y}{l}\right) \tag{13}$$

It is found from Eqn.(13) that $s_{\mathrm{p}}(y)$ is an odd function with respect to the coordinate y:

$$s_{\mathrm{p}}(-y)=-s_{\mathrm{p}}(y) \tag{14}$$

At the center of ASB, i.e., y=0, the local plastic shear deformation is

$$s_{\mathrm{p}}(0)=0 \tag{15}$$

At the top of ASB, i.e., $y=w/2$, the local plastic shear deformation is

$$s_p\left(\frac{w}{2}\right)=\frac{w\gamma_c}{2}+\left(\bar{\gamma}_p-\gamma_c\right)\cdot\frac{w}{2}=\frac{w\bar{\gamma}_p}{2} \tag{16}$$

At the base of ASB, i.e., $y=-w/2$, the local plastic shear deformation is

$$s_p\left(-\frac{w}{2}\right)=-\frac{w\gamma_c}{2}-\left(\bar{\gamma}_p-\gamma_c\right)\cdot\frac{w}{2}=-\frac{w\bar{\gamma}_p}{2} \tag{17}$$

Thus, the relative plastic shear deformation is

$$s_p\left(\frac{w}{2}\right)-s_p\left(-\frac{w}{2}\right)=w\bar{\gamma}_p \tag{18}$$

Eqns.(7) and (13) show that the distribution of local plastic shear strain in ASB is highly nonuniform, and the distribution of local plastic shear deformation in ASB is highly nonlinear.

4 Parametric study

4.1 Effect of static shear strength

Fig.1 shows the influence of static shear strength A on the flow shear stress—average plastic shear strain curve (τ—$\bar{\gamma}_p$ curve), the critical plastic shear strain γ_c, the local plastic shear strain $\gamma_p(y)$ and deformation $s_p(y)$ in ASB with l=3.18 μm, B=500 MPa, C=0.014, m=1.03, n=0.26, T_m=1 790 K, ρ=7 850 kg/m^3, T_0=300 K, $\dot{\gamma}_0$=3 300 s^{-1}, c_p=473 J/(kg·K), $\dot{\gamma}$=11 000 s^{-1} and β=0.9.

It is found from Fig.1 that higher value of A leads to higher peak flow shear stress τ_{max} and lower γ_c. The γ_c—A curve is concave upward. Fig.1(c) shows that higher A results in steeper profile of $\gamma_p(y)$ and higher peak local plastic shear strain $\gamma_{p,\,max}$, as also seen from Eqns.(7) and (8). This means that the distribution of $\gamma_p(y)$ becomes more nonuniform and the concentration of plastic shear strain in ASB becomes more apparent as A increases.

According to Eqn.(9), the local plastic shear strain at the two boundaries of ASB is equal to γ_c. Higher γ_c is expected at lower value of A, as seen from Figs.1((a)–(c)).

As can be seen from Fig.1(d), the distribution of $s_p(y)$ in ASB is nonlinear. The extent of the nonlinear distribution is more and more apparent at higher A. As seen from Fig.1(d) or Eqns.(15) and (18), the local plastic

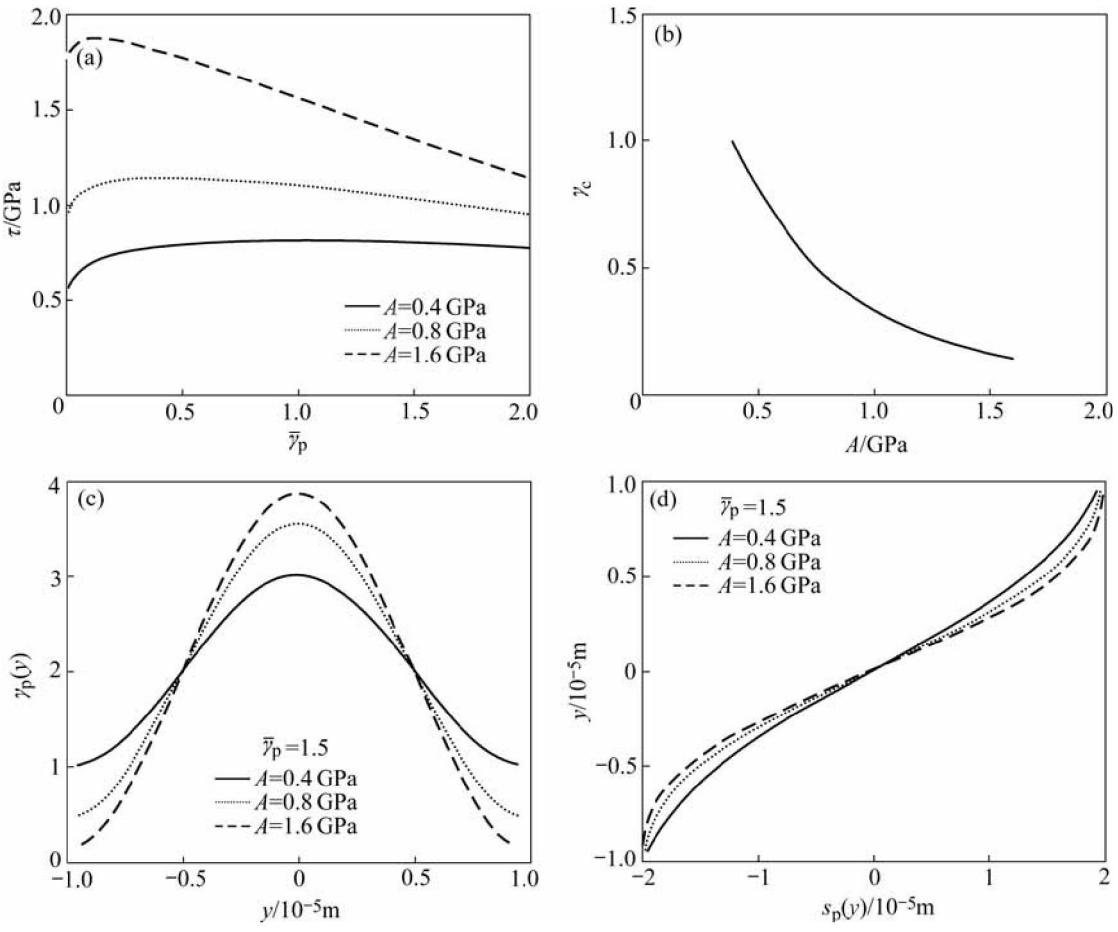

Fig.1 Effects of static shear strength A on flow shear stress—average plastic shear strain curve (a), critical plastic shear strain (b), local plastic shear strain (c) and deformation (d) in ASB

shear deformation at the center of ASB is zero, and the relative plastic shear deformation between the two ends of ASB is only dependent on the average plastic shear strain $\bar{\gamma}_p$ and the thickness w of ASB.

4.2 Effect of strain-hardening modulus

The effect of parameter B on τ—$\bar{\gamma}_p$ curve, γ_c, $\gamma_p(y)$ and $s_p(y)$ is shown in Fig.2 with l=3.18 μm, A=800 MPa, C=0.014, m=1.03, n=0.26, T_m=1 790 K, ρ=7 850 kg/m^3, T_0=300 K, $\dot{\gamma}_0$=3 300 s^{-1}, c_p=473 J/(kg·K), $\dot{\gamma}$=11 000 s^{-1} and β=0.9.

It can be found from Fig.2 that higher value of B leads to higher τ_{max}. As can be seen from Fig.2, higher γ_c is expected at higher B. Moreover, the γ_c—B curve is concave downward.

Fig.2(c) shows that lower B causes the profile of $\gamma_p(y)$ to be steeper; lower B results in higher $\gamma_{p,\,max}$ and lower γ_c, as also seen from Eqns.(8) and (9). From Fig.2(d), the profile of $s_p(y)$ is more curved at lower B.

It is noted that the γ_c—B curve is omitted in Fig.2(b) when B>1 GPa. It is found from numerical calculation that when B exceeds a critical value, γ_c decreases as B increases. Thus, for much higher B, $\gamma_{p,\,min}$(equal to γ_c) will be lower and $\gamma_{p,\,max}$ will be higher. Moreover, the profile of $\gamma_p(y)$ will be steeper and the distribution of $s_p(y)$ will be more curved.

4.3 Effect of sensitive coefficient of strain rate

The effect of parameter C on τ—$\bar{\gamma}_p$ curve, γ_c, $\gamma_p(y)$ and $s_p(y)$ is shown in Fig.3 with l=3.18 μm, B=500 MPa, A=800 MPa, m=1.03, n=0.26, T_m=1 790 K, ρ=7 850 kg/m^3, T_0=300 K, $\dot{\gamma}_0$=3 300 s^{-1}, c_p=473 J/(kg·K), $\dot{\gamma}$=11 000 s^{-1} and β=0.9.

Figs.3(a) and (b) show that higher τ_{max} is reached at higher value of C. γ_c slightly decreases as C increases so that the distributions of $\gamma_p(y)$ and $s_p(y)$ overlap for different values of C, as shown in Figs.3(c) and (d).

4.4 Effect of strain-hardening exponent

The effect of parameter n on τ—$\bar{\gamma}_p$ curve, γ_c, $\gamma_p(y)$ and $s_p(y)$ is shown in Fig.4 with l=3.18 μm, B=500 MPa, A=800 MPa, m=1.03, C=0.014, T_m=1 790 K, ρ=7 850 kg/m^3, T_0=300 K, $\dot{\gamma}_0$=3 300 s^{-1}, c_p=473 J/(kg·K), $\dot{\gamma}$=11 000 s^{-1} and β=0.9.

Figs.4(a) and 4(b) reveal that the higher the parameter n is, the higher τ_{max} and γ_c are. The γ_c—n curve

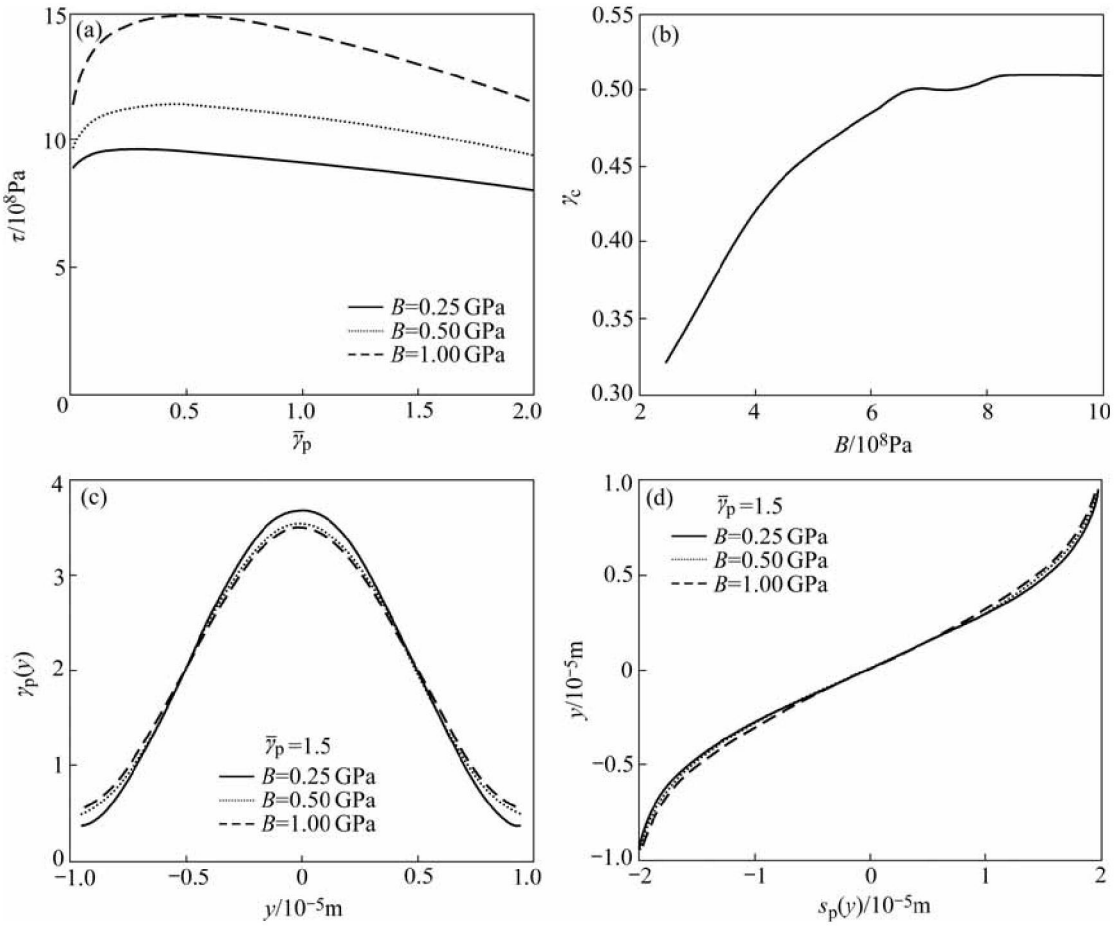

Fig.2 Effects of strain-hardening modulus B on flow shear stress—average plastic shear strain curve (a), critical plastic shear strain (b), local plastic shear strain (c) and deformation (d) in ASB

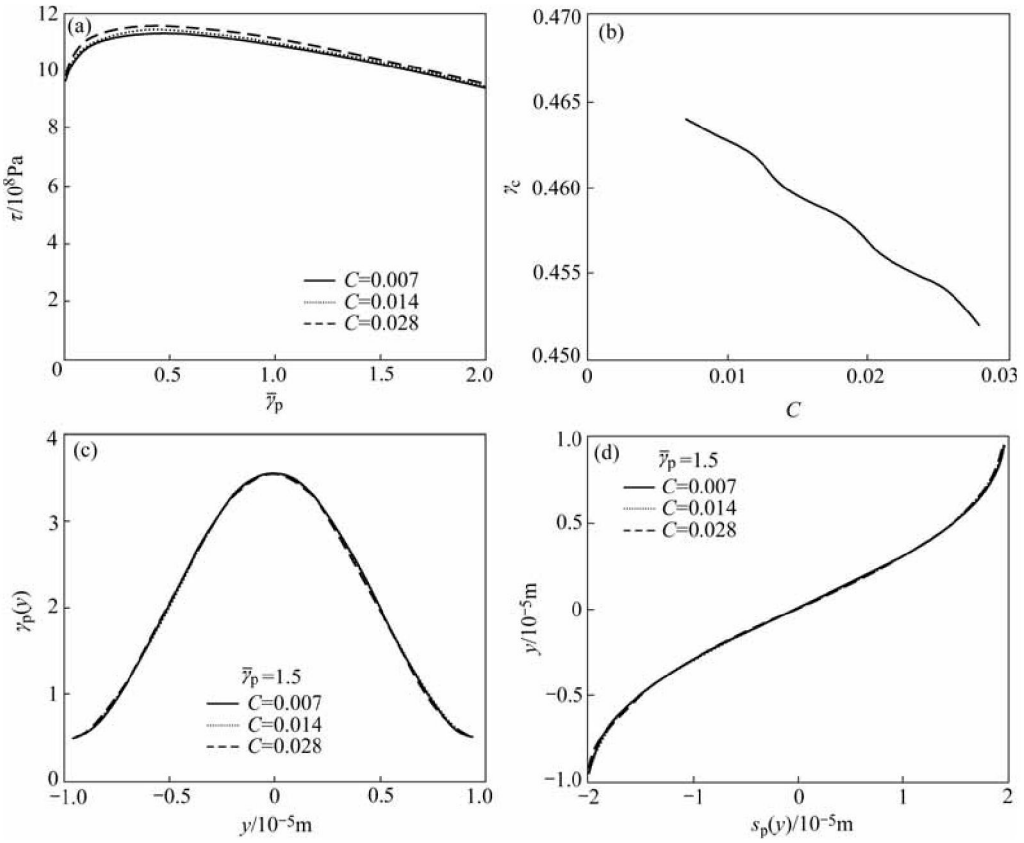

Fig.3 Effects of strain rate sensitive coefficient C on flow shear stress—average plastic shear strain curve (a), critical plastic shear strain (b), local plastic shear strain (c) and deformation (d) in ASB

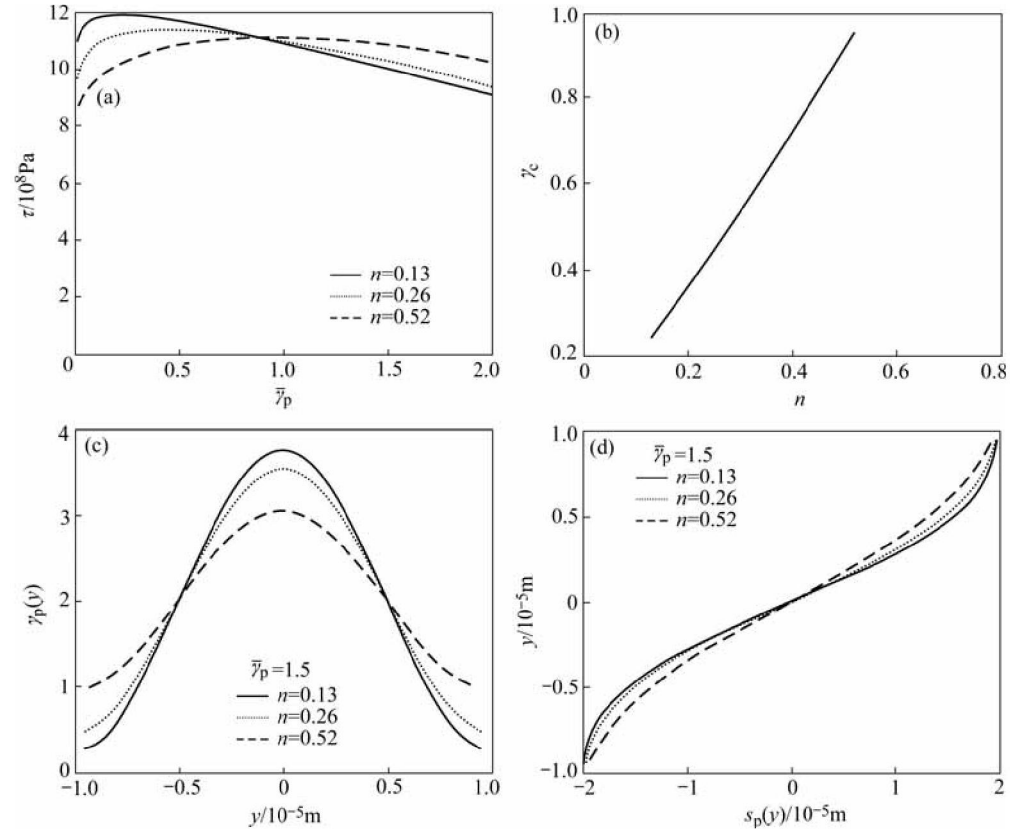

Fig.4 Effects of strain-hardening exponent n on flow shear stress—average plastic shear strain curve (a), critical plastic shear strain (b), local plastic shear strain (c) and deformation (d) in ASB

is approximately linear.

From Figs.4(c) and 4(d), it can be seen that the effect of n on $\gamma_p(y)$ and $s_p(y)$ is similar to the influence of B (less than a critical value), as shown in Figs.2(c) and 2(d).

4.5 Effect of thermal-softening coefficient

The effect of parameter m on τ—$\bar{\gamma}_p$ curve, γ_c, $\gamma_p(y)$ and $s_p(y)$ is shown in Fig.5 with l=3.18 μm, B=500 MPa, A=800 MPa, n=0.26, C=0.014, T_m=1 790 K, ρ=7 850 kg/m^3, T_0=300 K, $\dot{\gamma}_0$ =3 300 s^{-1}, c_p=473 J/(kg·K), $\dot{\gamma}$ =11 000 s^{-1} and β=0.9.

Fig.5(a) shows that higher m causes τ_{max} to be higher. Fig.5(b) reflects that γ_c is linearly increased with the increase of m.

It can be seen from Figs.5(c) and 5(d) that the effect of m on $\gamma_p(y)$ and $s_p(y)$ is very similar to the effects of n and B (less than a critical value), as shown in Figs.4(c) and (d), Figs.2(c) and (d), respectively.

4.6 Effect of melting point

The effect of parameter T_m on τ—$\bar{\gamma}_p$ curve, γ_c, $\gamma_p(y)$ and $s_p(y)$ is shown in Fig.6 with l=3.18 μm, B=500 MPa, A=800 MPa, n=0.26, C=0.014, m=1.03, ρ=7 850 kg/m^3, T_0=300 K, $\dot{\gamma}_0$ =3 300 s^{-1}, c_p=473 J/(kg·K), $\dot{\gamma}$ =11 000 s^{-1} and β=0.9.

It can be seen from Figs.6((a)−(b)) that higher T_m leads to higher τ_{max} and γ_c.

It can be seen from Figs.6((c)−(d)) that the influence of T_m on $\gamma_p(y)$ and $s_p(y)$ is similar to the effects of m, n and B (less than a critical value), as can be seen from Figs.5((c)− (d)), Figs.4((c)−(d)) and Figs.2((c)−(d)), respectively.

4.7 Effects of heat capacity, density and work to heat conversion factor

The effect of parameter c_p on τ—$\bar{\gamma}_p$ curve, γ_c, $\gamma_p(y)$ and $s_p(y)$ is shown in Fig.7 with l=3.18 μm, B=500 MPa, A=800 MPa, n=0.26, C=0.014, m=1.03, ρ=7 850 kg/m^3, T_0=300 K, $\dot{\gamma}_0$ =3 300 s^{-1}, T_m=1 790 K, $\dot{\gamma}$ =11 000 s^{-1} and β=0.9.

Eqn.(2) shows that ρ and c_p are denominator while β is numerator. Consequently, the influence of ρ and c_p is similar and the effects of c_p and β are opposite.

It is found from Figs.7 ((a)−(b)) that higher c_p leads to higher τ_{max} and γ_c.

Figs.7((a)−(b)) show that the influence of c_p on $\gamma_p(y)$ and $s_p(y)$ is similar to the effects of parameters T_m, m, n

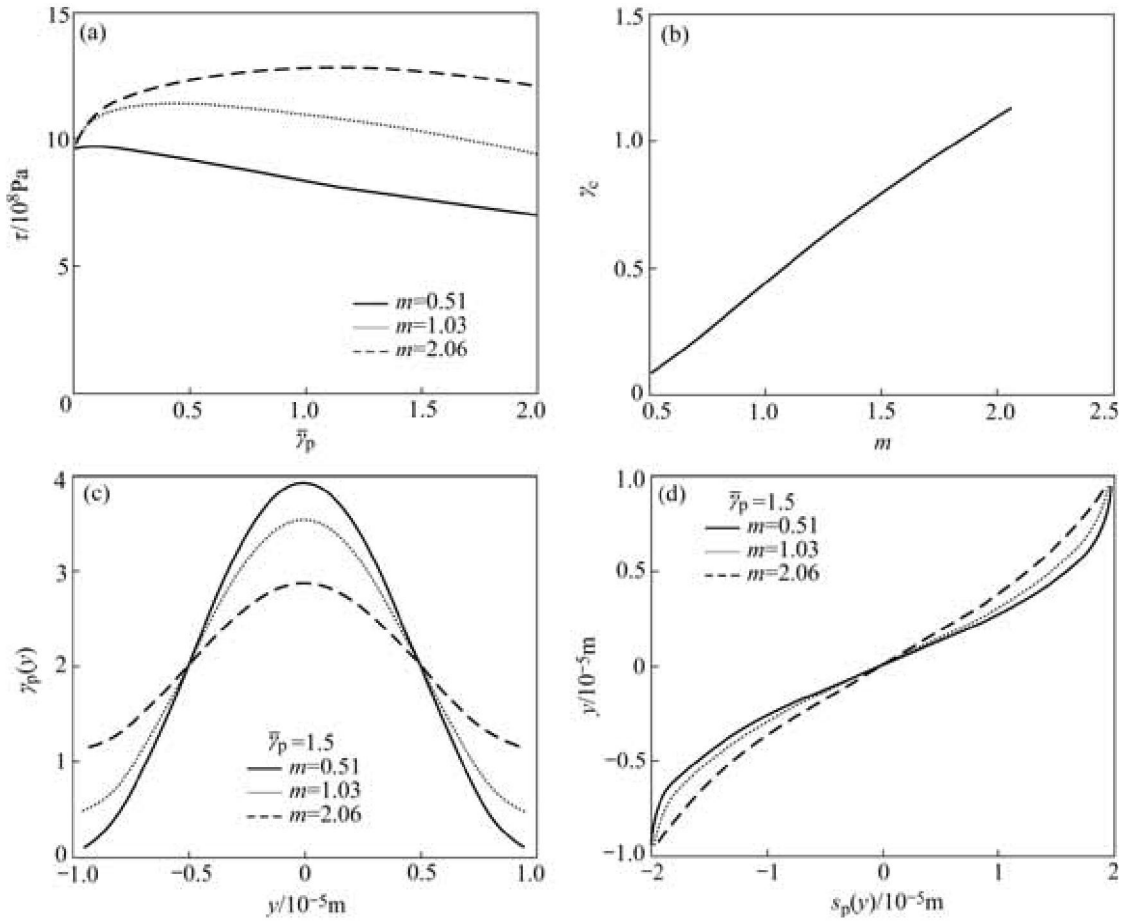

Fig.5 Effects of thermal-softening exponent m on flow shear stress—average plastic shear strain curve (a), critical plastic shear strain (b), local plastic shear strain (c) and deformation (d) in ASB

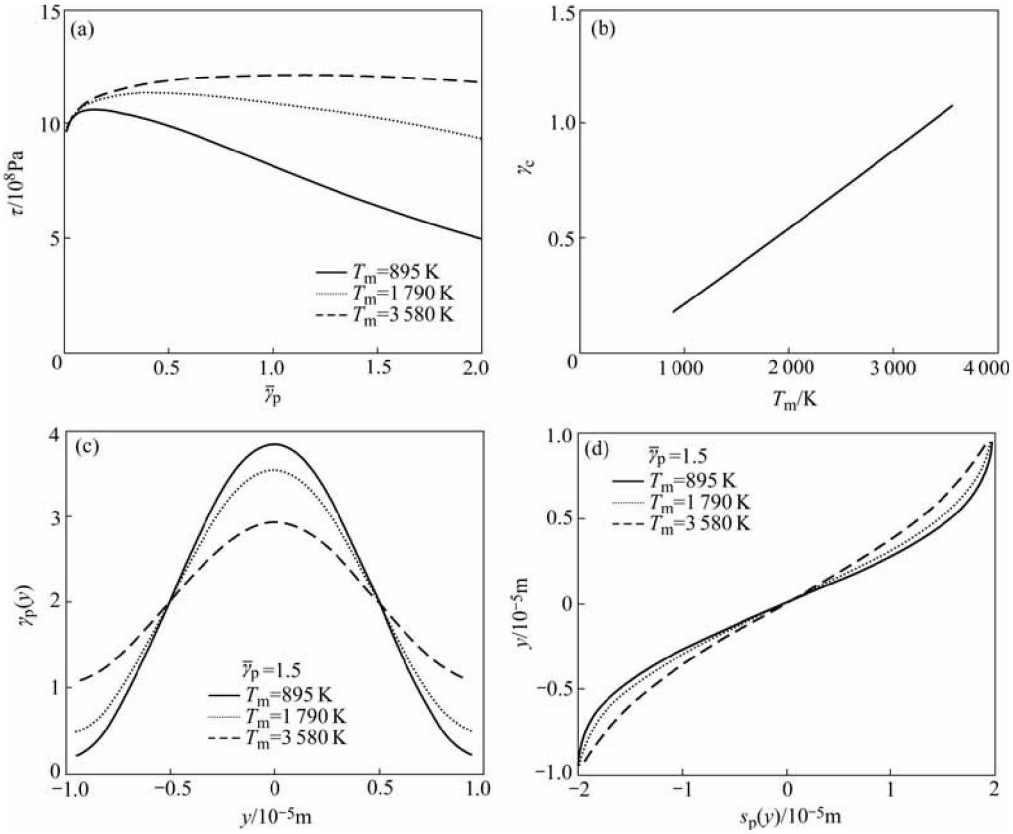

Fig.6 Effects of melting point T_m on flow shear stress—average plastic shear strain curve (a), critical plastic shear strain (b), local plastic shear strain (c) and deformation (d) in ASB

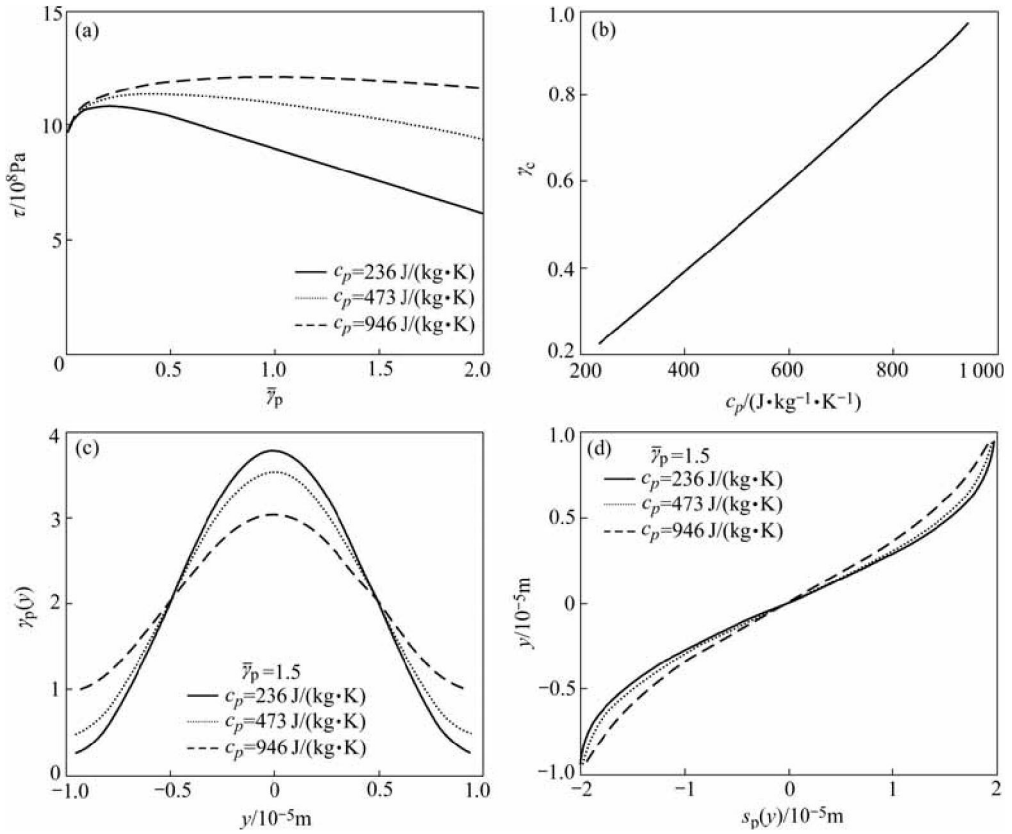

Fig.7 Effects of thermal capacity c_p on flow shear stress—average plastic shear strain curve (a), critical plastic shear strain (b), local plastic shear strain (c) and deformation (d) in ASB

and B (less than a critical value), as it can be seen from Figs.6((c)−(d)), Figs.5((c)−(d)), Figs.4((c)−(d)) and Figs.2(c)−(d)), respectively.

5 Conclusions

1) The peak local plastic shear strain is proportional to the average plastic shear strain, while it is inversely proportional to the critical plastic shear strain corresponding to the peak flow shear stress. The relative plastic shear deformation between the top and base of ASB is only dependent on the thickness of ASB and the average plastic shear strain.

2) Effects of constitutive parameters, such as static shear strength, strain-hardening modulus, strain-hardening exponent, strain rate sensitive coefficient, thermal-softening exponent, melting point, thermal capacity, mass density and work to heat conversion factor, on the flow shear stress—average plastic shear strain curve, the critical plastic shear strain, the distributions of local plastic shear strain and deformation in ASB are investigated by a detailed parametric study.

3) Higher static shear strength and work to heat conversion factor lead to lower critical plastic shear strain so that shear localization is more apparent at the same average plastic shear strain. Higher strain-hardening exponent, strain rate sensitive coefficient, melting point, thermal capacity and mass density result in higher critical plastic shear strain, leading to less apparent shear localization at the same average plastic shear strain. The strain rate sensitive coefficient has a minor influence on the critical plastic shear strain, the distributions of local plastic shear strain and deformation in ASB. At a critical value of strain-hardening modulus, the critical plastic shear strain is maximum, leading to the least apparent shear localization.

References

[1] BAI Y, BODD B, Adiabatic Shear Localization [M]. Oxford: Pergamon Press, 1992.

[2] LEECH P W. Observations of adiabatic shear band formation in 7039 aluminum-alloy [J]. Metallurgical Transactions A, 1985, A16(10): 1900−1903.

[3] XU Y B, ZHONG W L, CHEN Y J, SHEN L T, LIU Q, BAI Y L, MEYERS M A. Shear localization and recrystallization in dynamic deformation of 8090 Al-Li alloy [J]. Materials Science and Engineering A, 2001, A299(1/2): 287−295.

[4] LEE C G, LEE Y J, LEE S H. Observation of adiabatic shear bands formed by ballistic impact in aluminum-lithium alloys [J]. Scripta Metallurgica et Materialia, 1995, 32(6): 821−826.

[5] LIAO S C, DUFFY J. Adiabatic shear bands in a Ti-6Al-4V Titanium alloy [J]. J Mech Phys Solids, 1998, 46(11): 2201−2231.

[6] ZHOU M, ROSAKIS A J, RAVICHANDRAN G. Dynamically propagating shear bands in impact-loaded prenotched plates-I. Experimental investigations of temperature signatures and propagation speed [J]. J Mech Phys Solids, 1996, 44(6): 981−1006.

[7] YANG Yang, XIONG Jun, YANG Xu-yue. Microstructure evolution mechanism in adiabatic shear band in TA2 [J]. Trans Nonferrous Met Soc China, 2004, 14(4): 670−674.

[8] ME-BAR Y, SHECHTMAN D. On the adiabatic shear of Ti-6Al-4V ballistic targets [J]. Materials Science and Engineering, 1983, 58(2): 181−188.

[9] MOLINARI A, MUSQUAR C, SUTTER G. Adiabatic shear banding in high speed machining of Ti-6Al-4V: experiments and modeling [J]. International Journal of Plasticity, 2002, 18(4): 443−459.

[10] XUE Q, MEYERS M A, NESTERENKO V F. Self-organization of shear bands in titanium and Ti-6Al-4V alloy [J]. Acta Mater, 2002, 50(3): 575−596.

[11] YANG Y, WANG B F, HU B, HU K, LI Z G. The collective behavior and spacing of adiabatic shear bands in the explosive cladding plate interface [J]. Materials Science and Engineering A, 2005, A398(1/2): 291−296.

[12] KLEPACZKO J R, REZAIG B. A numerical study of adiabatic shear banding in mild steel by dislocation mechanics based constitutive relations [J]. Mech Mater, 1996, 24(2): 125−139.

[13] DARIDON L, OUSSOUADDI O, AHZO S. Influence of the material constitutive models on the adiabatic shear band spacing: MTS, power law and Johnson-Cook models [J]. Int J Solids Struct, 2004, 41(11−12): 3109−3124.

[14] BATRA R C, LEAR M H. Adiabatic shear banding in plane strain tensile deformations of 11 thermoelastoviscoplastic materials with finite thermal wave speed [J]. International Journal of Plasticity, 2005, 21(8): 1521−1545.

[15] RAVICHANDRAN G, MOLINARI A. Analysis of shear banding in metallic glasses under bending [J]. Acta Materialia, 2005, 53(15): 4087−4095.

[16] WANG Xue-bin. Calculation of temperature distribution in adiabatic shear band based on gradient-dependent plasticity [J]. Trans Nonferrous Met Soc China, 2004, 14(6): 1062−1067.

[17] WANG X B. Local and global damages of quasi-brittle material in uniaxial compression based on gradient-dependent plasticity [J]. Key Eng Mater, 2005, 293−294: 719−726.

[18] WANG Xue-bin, DAI Shu-hong, HAI Long, PAN Yi-shan. Analysis of localized shear deformation of ductile metal based on gradient-dependent plasticity [J]. Trans Nonferrous Met Soc China, 2003, 13(6): 1348−1353.

[19] WANG Xue-bin, YANG Mei, YU Hai-jun, HAI Long, PAN Yi-shan. Localized shear deformation during shear band propagation in titanium considering interactions among microstructures [J]. Trans Nonferrous Met Soc China, 2004, 14(2): 335−339.

[20] WANG Xue-bin, YANG Mei, ZHAO Yang-feng. Analytical solution for true stress-true strain curve for titanium and Ti-6Al-4V in uniaxial tension considering interaction among microstructures [J]. Rare Metal Materials and Engineering, 2005, 34(3): 346−349. (in Chinese)

[21] WANG Xue-bin, YANG Mei. Analysis of percent elongation for ductile metal in uniaxial tension considering interactions among microstructures [J]. Journal of Iron and Steel Research, International, 2005, 12(3): 34−39.

[22] WANG Xue-bin. Temperature distribution in adiabatic shear band for ductile metal based on Johnson-Cook and gradient plasticity models [J]. Trans Nonferrous Met Soc China, 2006, 16(2): 333−338.

(Edited by LI Xiang-qun)